Thermal Design of an Integrated Inductor for 45kW Aerospace Starter-Generator

A. La Rocca, M. Raza Khowja, G. Vakil, C. Gerada, P. Wheeler, Lyan*
Power Electronics, Machines and Control (PEMC) Group
The University of Nottingham, UK
*School of Automation science and Electrical Engineering
Beihang University, Beijing, China.
Email: a.larocca@nottingham.ac.uk, raza.khowja@ottingham.ac.uk, gaurang.vakil@nottingham.ac.uk, christopher.gerada@nottingham.ac.uk, pat.wheeler@nottingham.ac.uk, lyan1991@gmail.com

***Abstract*- This paper presents a combined electromagnetic and thermal design of integrated inductor, for the application of a 45kW aircraft starter-generator. The inductor is designed at high current density by using the apporach ofarea product, followed by the finite element analysis, which validates the electromagnetic performance of integrated inductor. The total power losses at 8, 20, and 32kRPM are evaluated in order to investigate the thermal design of a combined starter-generator and integrated inductor system, whilst, achieving the full integration from a thermal management point of view. As both starter/generator and inductor share common cooling configuration; performance of a direct and an indirect cooling options are compared. The direct cooling configuration, based on a semi-flooded design, can lead to a temperature reduction up to 90°C in the most critical components.**

***Index Terms* —Integrated Inductor, Integration of Passives, Rotor-less Inductor, Thermal Design and Starter-Generator.**

I. INTRODUCTION

A compact motor drive system is required, from physical and functional integration point of view, in order to achieve higher power density and efficiency. Such power dense systems are mandatory in aircraft, marine and transportation applications. Passive elements which are introduced after the drive components have been defined lead into discrete sub-systems [1]. To overcome this, the integration of passives need to be introduced both from functional and physical point of view [2, 3]. There are many possibilities in the aircraft motor-drive systems to integrate the passive components. Pasives integration in such systems offer many advantages such as increased energy densities, reduced price, weight, space and eases the construction task. Thus, applications where high energy densities are required, integrative approach appears to be the best solution [4, 5]. In the past, the integration of passives has been a focus in electric motor drive market that has resulted in an overall compact design of a power system. In [2, 3], a new integration methodology of the inverter output filter inductor is presented for permanent magnet synchronous motor drive systems. Integrated motor uses the main motor inductance as filter inductance instead of sizing a separate inductor between the inverter and the motor, which yields to the elimination of ohmic losses and its associated mass and occupied space. The author of [4-7] introduced two new options for passive filter inductors integrated within the common housing of the motor

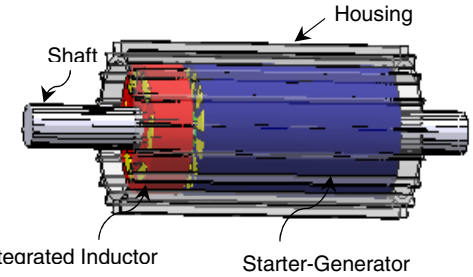

Fig. 1. Radial Cross-section and Flux Distribution (a) EE Core Inductor

as shown in Fig. 1. It includes: motor-shaped rotational inductor and motor-shaped rotor-less inductor. Both integrated inductors are mounted axially on to the rotor shaft, resulting in a shared cooling system. Thus, eliminating the requirement of an external cooling system. The rotor of the rotational inductor rotates with the fundamental freuqncy of the stator magnetic field which minimises the rotor iron losses. On the other hand, integrated rotor-less inductor has the identical structure, but without rotor, which makes it appropriate for smoothing inductors for DC-Link applications, grid-side input filters and isolation transformers. In comparison, the rotational inductor can only be employed for high speed motor drive systems. In [8], author has presented a design of motor-shaped rotor-less inductor adopted for 45kW aircraft starter-generator. This integrated inductor was designed and sized at current density of 18A/mm^2 which uses the existing cooling system of the starter-generator. A substantial weight and space reduction of 55.4% and 52.7 respectively is achieved, when compared with the standard EE-core inductor which had come at the expense of higher ohmic losses, where, heat generated in the windings is assumed to be taken out by the cooling system available for the starter-generator, designed for aircraft applications.

This paper presents the thermal investigation of an integrated rotor-less inductor proposed in [8] which is adopted for a 45kW aerospace starter-generator. In the next section, design procedure of the inductor using area product approach is discussed. Section III provides the detail of the starter-generator that requires a series inductor to be added with its main windings, in order to improve current and torque ripple. In section IV, sizing of the integrated inductor is discussed, followed by the thermal analysis of the starter-generator combined with an integrated inductor in section V.

II. Area Product Approach

The voltage due to electromagnetic induction, accross the terminals of an inductor, can be obtained by referring Fig. 2 if the supply current and voltage across the inductor is sinosoildal. Therefore, the induced voltage is given by,

$$V_{pk} = N_{phase}\varphi_{pk}\omega_{supply} \quad (1)$$

$$V_{rms} = K_w N_{phase} B_{pk} A_{core} f_{supply} \quad (2)$$

Where K_w , A_c. φ_{pk}, B_{pk}, f_{supply} and N_{phase} are waveform factor, iron core cross-section area, magnetic flux created by the electromagnetic field, peak value of flux density, supply frequency and the phase turns respectively. The turns per phase of the inductor, for a given conductor and window area can be determined by,

$$N_{phase} = \frac{K_F W_a}{A_{st}} \quad (3)$$

Where, K_F is the window utilisation factor In general, for inductor, window utilisation factor typically varies from 0.45 to 0.55 in order to provide enough space for bobbins, slot liner and the wire insulation [8]. By substituting (3) in (2), we have,

$$V_{rms} = \frac{K_F K_w B_{pk} A_{core} W_a f_{supply}}{A_{st}} \quad (4)$$

By multiplying I_{rms} eon both sides, we have,

$$V_{rms} I_{rms} = \frac{K_F K_w B_{pk} A_{core} W_a f_{supply} I_{rms}}{A_{st}} \quad (5)$$

Solving for the area product, we have,

$$A_{core}.W_a = A_{p,1ph} = \frac{V_{rms} I_{rms}}{K_F K_w B_{pk} J_{rms} f_{supply}} \quad (6)$$

$$A_{core}.W_a = A_{p,1ph} = \frac{2\pi\, I_{rms}^2 L_{synch}}{K_F K_w B_{pk} J_{rms}} \quad (7)$$

Where J_{rms} is the RMS current density of the copper conductor which is limited by thermal loading of the inductor windings. For 3-phase inductors the area product changes to,

$$A_{p,3ph} = 3A_{core}.\left(\frac{W_a}{2}\right) = 1.5A_{p,1ph} \quad (8)$$

From (6), it can be observe that the parameters such as window utilisation factor, magnetic flux density and conductor current density has an influence on the inductor's area product. The left hand side shows the physical parameters of an inductor, whereas, the right hand side shows the parameters that depends on the electrical and magnetic loading of an inductor. The core area narrates the flux permeance capacity, whereas, the window area defines inductor's current conduction capacity [4-9]. It is important to note that the area product does not depend on the fundamental supply frequency. But, the iron losses depends on the frequency squared. Hence, when designing an inductor for high frequency (kHz to MHz) applications, it is necessary to consider the flux density inside iron core is adjusted to a lower value when compared to indcutor designed for low frequency (Hz to kHz) applications [8, 9].

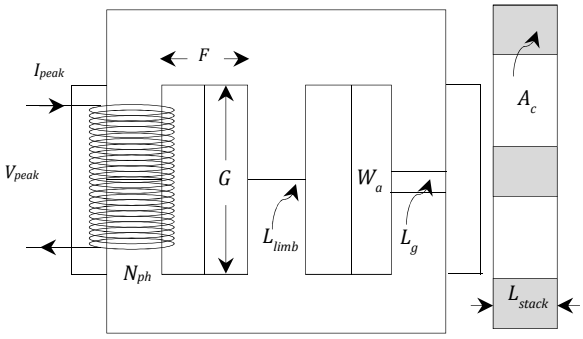

Fig. 2. Physcial Layout of 3 Phase EE core Inductor

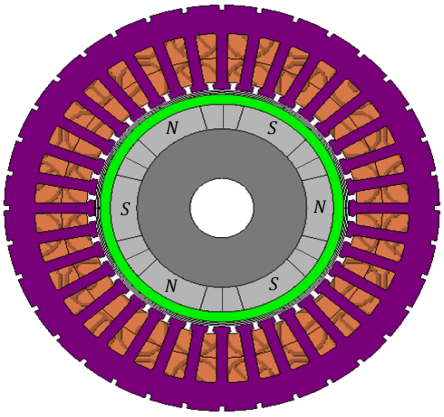

Fig. 3. Radial Corss-section of the Starter-Generator

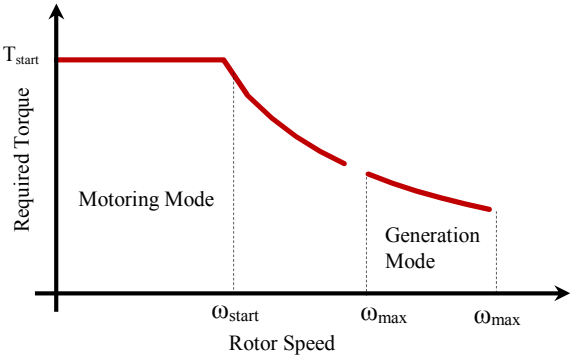

Fig. 4. Torque-speed Characteristics of the Starter-Generator

III. 45kW Aeropsace Starter-Generator

The circumferential cross-section and torque-speed curve of the starter-generator, used for aircraft application, are shown in Fig. 3 and Fig. 4 respectively, the key parameters of which are illustrated in Table I. The starter-generator works as a motor during engine start and is required to produce a constant power (or torque) from standstill to an engine firing speed of 8 kRPM. Between the speeds of 8 kRPM (ω_{start}) to 20 kRPM (ω_{min}), the starter-generator feeds the constant power to accelerate the engine. Once the engine reaches its steady state region, the starter-generator turned into a generation mode between the speeds of 20 kRPM (ω_{min}) and 32 kRPM (ω_{max}).

In generation mode, the starter-generator induces output power of 45kW up to a maximum speed of 32 kRPM (ω_{max}). Since the phase inductance of the starter-generator is very low (99 µH), an additional inductance is needed to increase the main inductance of the starter-generator, by twice. This increase in inductance will reduce the magnitude of switching current component by half through the starter-generator. Furthermore, doubling the motor's main inductance will help the control system to be designed at lower switching frequency [8].

TABLE I.
DESIGN DETAILS OF THE STARTER-GENERATOR

PARAMETERS	VALUE	UNIT
Iron Material (Stator Core)	Hiperco 50	-
Slot and Pole Number	6 slot/2 pole	-
Cooling System	Liquid/Oil	-
Base Speed	8000	RPM
Max. Speed	32,000	RPM
Current at 8000 RPM	236.9	A_{rms}
Current at 20,00 RPM	154.4	A_{rms}
Current at 32,000 RPM	188.2	A_{rms}
Current Density	18	A_{rms}/mm^2
Stack Length (Active)	80.2	mm
Outer and Inner Diameter	164/96	mm
Shaft Diameter	4	mm
Phase Resistance @ 30 ^{0}C	13.2	mΩ
Phase Inductance	99	µH

TABLE II.
REQUIRED SPECIFICATIONS OF INTEGRATED INDUCTOR

SPECIFICATIONS	VALUES	UNIT
Iron Material (Stator Core)	Hiperco 50A	-
Required Inductance	99	µH
Rated Current	236.9	A_{rms}
Max. Flux Density	2.3	T
Slot Utilisation Factor	0.5	-
Current Density	18.0	A_{rms}/mm^2
Waveform Factor (K_w)	4.44	-

IV. SIZING OF INTEGRATED INDUCTOR

6 slots 2 poles integrated rotor-less inductor, with double layer concentrated winding (DL CNW), is selected to design at current density of 18A/mm^2 (same as the current density of the starter-generator). The main reason of choosing DL CNW is to restrict overall volume of the end-windings which was the stringent requirement of the starter-generator system. In order to size the integrated inductor area product approach is used, as discussed in section II. The integrated inductor is sized by specifying the required filter inductance, maximum magnetic flux density, window utilisation factor, conductor current density and the type of stator core material, the details of which are shown in Table II. While sizing an inductor, the following design ratios were presumed: window area to core area ratio (W_a/A_{core}) is 0.7, window length to height ratio (G/F) is 3 and stack length to limb length ratio (L_{stack}/L_{limb}) is 0.77 [8].

The author of [9, 10] has recommended to assume a low window-to-core area ratio (W_a/A_{core}) to keep the fringing effect at smallest level. Also, the window length-to-height ratio is selected, based on the information provided by the manufacturer in [9]. However, the stack-to-limb ratio is chosen

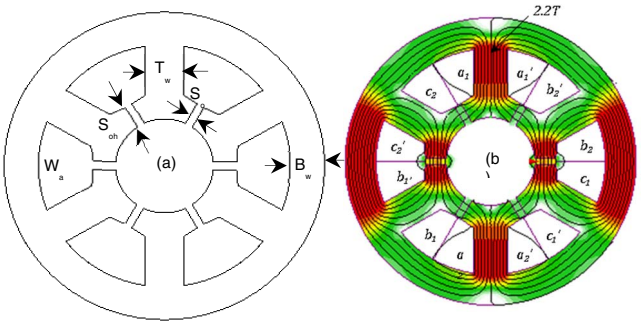

Fig. 5. Intergrated Rotor-less inductor (a)Physical Layout (b) Flux distribution

TABLE III.
POWER LOSSES OF INTEGRATED INDUCTOR AND STATER-GENERATOR

Rotor Speed (RPM)	Starter-Generator (Iron + Copper), kW	Integrated Inductor (Iron + Copper), kW
8000	0.238 + 2.625	0.092 + 2.135
20,000	0.124 + 0.952	0.169 + 0.668
32,000	0.206 + 1.424	0.458 + 0.998

based on the dimensions (i.e. outer diameter) limitation of the starter-generator. At first, the inductor's area product is calculated based on (7) and (8) using the parameters, as shown in Table II. The window area and the core area are calculated using the area product and the assumed window-to-core area ratio ratio. Once the window area and core area are evaluated, the core length ratio (L_{stack}/L_{limb}) and window aspect ratio (G/F) are then chosen to fix the tooth width, stack length, window width and window height. The back iron width and slot opening height are adjusted until the required flux density is achieved in the core (which is in the range of 2.2T to 2.3T). The number of turns per phase are computed based on the specified voltage across the inductor [8].

$$N_{phase} = \frac{V_{rms}}{K_F A_{core} B_{pk} f_{supply}} \quad (6)$$

Once the inductor is designed, the FE model is built using the commercially available software "MagNet by Infolytica". Fig. 5(a) and Fig. 5(b) shows the physical layout and flux distribution of the integrated rotor-less inductor respectively. The inductance value of 90µH is obtained from FEA model as oppose to the required inductance of 99µH. In order to achieve the filter inductance of 99µH, the inductor's stack length is adjusted from 20mm to 22.5mm. The end winding overhang is estimated using the method explained in [6, 7], giving a total inductor axial length of 46.5mm [8].

The ohmic copper losses evaluated from FE at all three speeds are illustrated in Table III, for both starter-generator and integrated inductor. It can be seen that the worst case scenario in terms of total power losses is at the speed of 8000 RPM, where, both starter-generator and inductor dissipates the maximum amount of heat. Therefore, it is a straightforward decision to pick the speed of 8000 RPM for thermal investigation of a combined starter-generator and integrated inductor system.

V. THERMAL DESIGN

In order to achieve a fully integrated solution it was decided to also have an integrated cooling configuration. Two cooling strategies were considered, one indirect and one direct. The direct option implies the use of a standard helicoidal water jacked within the outer housing of both starter/generator and inductor; the heat is expected to be primarily dissipated by conduction through the housing, whilst a smaller amount will be dissipated into the end region due to the turbulent flow induced by the rotation itself. Figure 6 shows the configuration described.

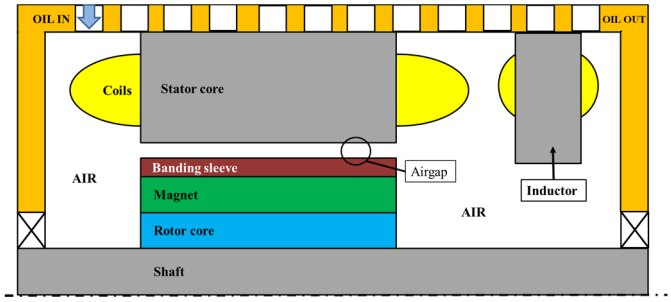

Fig. 6: Schematic of Indirect Integrated Cooling Design

The channel within the housing was assumed to be 10x3 mm, based on that a heat transfer coefficient of 1,400 W/m^{2}K was estimated using the empirical correlation (10) [11]; this value could be then used as boundary condition in the models developed.

$$Nu = 0.0059\, Re^{0.92} Pr^{0.4} \tag{10}$$

The convective heat transfer coefficients used on the internal surfaces of the machines, took into account the turbulence generated by the rotation; in order to do that the following correlation (11) was used [12].

$$h = k_1\,[1 + k_2\, v^{k_3}] \tag{11}$$

Where v is the reference velocity which is the average velocity of the rotating surfaces and the terms k_1, k_2, k_3 are curve fit coefficients. In particular k_1 accounts for the component of the natural convection, whilst k_2 and k_3 account for the convection due to rotation.

The thermal behaviour of both components was predicted numerically by the means of a numerical tool such as ANSYS Fluent. 3D simulation were carried out and, in order to reduce the computational cost, only a limited angular sector was considered. Furthermore the two stages were analysed separately using appropriate boundary conditions. The power loss of the components was implemented as volumetric heat generation boundary condition. Values used were based on the electromagnetic predictions described above.

A worst case scenario was considered for the thermal analyses; that is the steady-state condition at the least efficient operating point which was identified to be at 8,000 rpm. Due to the negligible loss in the rotor, the rotating components were not included in the model. Table IV lists the power loss implemented.

TABLE IV:
S/G AND INDUCTOR POWER LOSSES AT 8,000 RPM

COMPONENT	Power Loss (W)
Iron (S/G)	238
Iron (Inductor)	92
Copper (S/G)	2,650
Copper (Inductor)	1,570

The anistotropic nature of the windings was accounted for in the model to achieve more realistic temperature gradients within the coil bundles; this was done assigning different values of thermal conductivity along each spatial direction. Those values could be determined by applying the cuboidal model, shown below (12), as described in [13].

$$k_{eq} = k_a \frac{(1+v_c)k_c + (1-v_c)k_a}{(1-v_c)k_c + (1-v_c)k_a} \tag{12}$$

Where the equivalent thermal conductivity value k_{eq} is function of the volume and thermal conductivity of the materials inside the slot, such as copper and insulation.

Figures 7 and 8 show the temperature distribution within both starter/generator and inductor assuming a water inlet temperature of the jacket at 40°C.

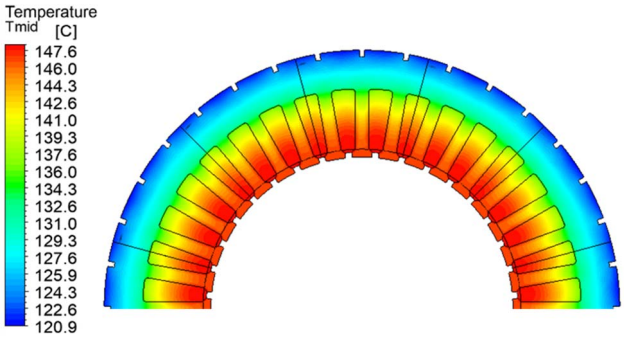

Fig.7: Temperature Distribution in the S/G with Water Jacket

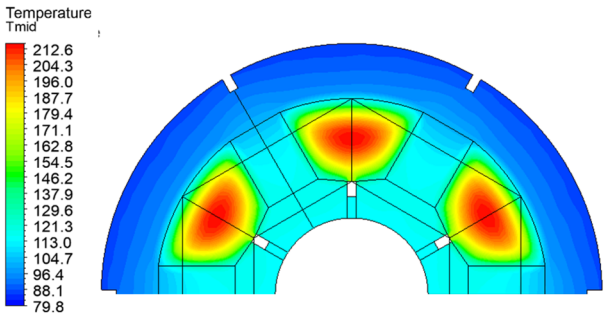

Fig. 8: Temperature Distribution in the Inductor with Water Jacket

As it can be noticed the temperature levels achieved exceed the allowable limits, making the water jacket not a viable option. For this reason a more intensive cooling option was assumed instead.

The direct cooling option adopted consist of a semi-flooded design where the coolant (oil) is directly in contact with all the stationary components. Non-electrically conductive sleeves

are used to contain the oil and to physically separate the stator region from the rotating components; this helps to keep the friction loss, generated due to viscous effects, as low as possible.

Such cooling option as already implemented in the starter generated and the performance fully validated as documented in [13]. Figure 9 show the schematic of the configuration described.

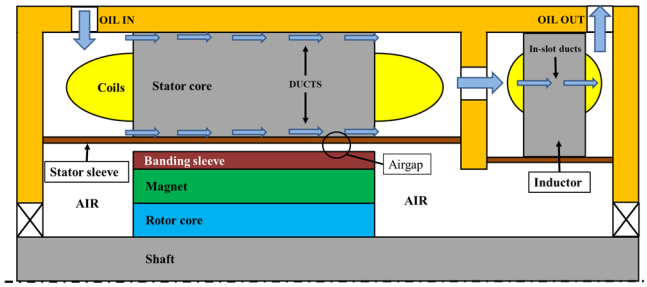

Fig.9: Schematic of Direct Integrated Cooling Design

The coolant flow through the first stage (starter/generator) through axial ducts located along the inner and outer diameter of the lamination as shown in Fig.4, following that the oil enters the inductor chamber and flows through 1.5 mm wide in-slot ducts, created in-between the concentrated windings, before leaving the system. Due to the gap created inside the slot, the copper losses had to be updated accordingly in order to take into account the lower fill factor; this led the power loss to increase to 2,135 W.

Figures 10 and 11 show the two designs of both starter/generator and inductor which were analysed.

In order to enhance the conductive heat transfer within the inductor, a sheet of ceramic material was located in the teeth opening; aluminium nitrate with a thermal conductivity of 100 W/mK was assumed. The thermal analyses carried out did not include any fluid domain, therefore some appropriate boundary conditions, based on previous works carried out [14], had to be implemented to take into account the convective heat transfer. A list of heat transfer coefficients used is shown in Table V below.

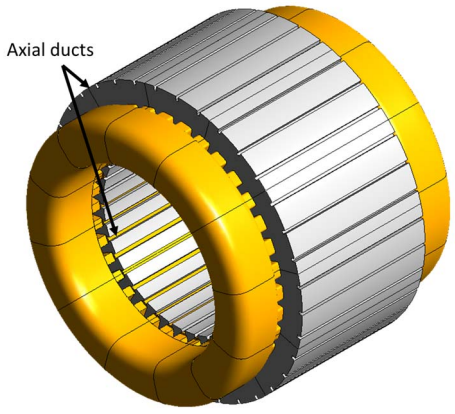

Fig. 10: Starter/Generator Domain

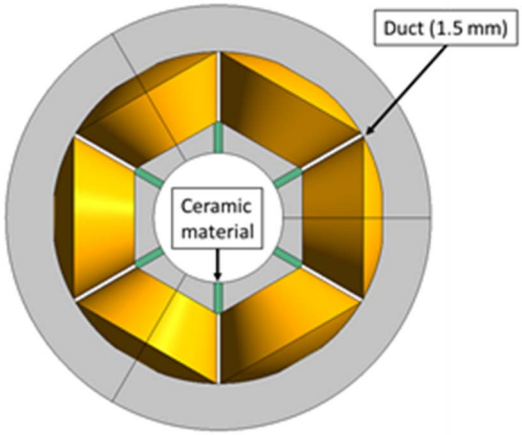

Fig. 11: Inductor Domain

TABLE V:
CONVECTIVE HEAT TRANSFER USED AS BOUNDARY CONDITIONS

SURFACE	**Heat transfer coefficient *h* (W/m²K)**
End-windings	900
Axial ducts (S/G)	800
Axial ducts (Inductor)	1,200
Lamination wet walls	400

The convective heat transfer in the axial ducts was additionally verified by analytical predictions based on an empirical correlation of the Nusselt number such as the one below (13) [14]. This correlation takes into account the fact that the fluid flow inside the duct is not fully developed for most of the length of the duct itself.

$$Nu = 3.65 + \frac{0.0668\,(d_h/l)Re\,Pr}{1 + 0.04\,[(d_h/l)\,Re\,Pr]^{2/3}} \qquad (14)$$

To determine the length of the entrance region within the duct the following expression (15) can be used.

$$X = 0.05\,Re\,d_h \qquad (15)$$

Where d_h is the duct hydraulic diameter.

The inlet temperature of the coolant at first stage (S/G) was set to be at 40°C whilst 46°C for the inductor. That takes into account the temperature increase due to the heat absorption. It was also assumed that all the losses were dissipated into the oil, so no any external convection was included; that provides a more conservative approach.

Figures 12 and 13 show the temperature contour plots of the starter/generator and inductor respectively, taken in the middle section, showing the highest temperatures achieved.

As results show, the shared semi-flooded configuration proposed allows maintaining the operating temperatures well below the maximum allowable limits, leaving a significant safety margin in case of over power conditions or short circuit failure conditions.

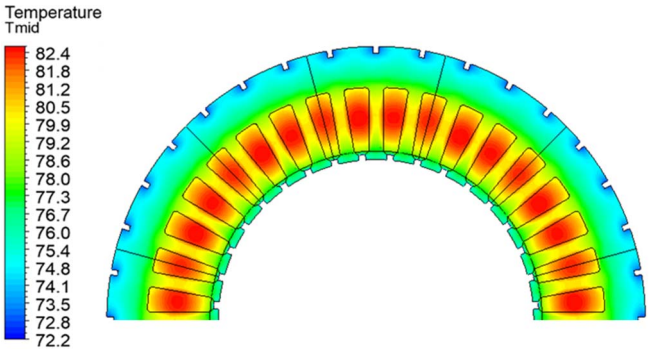

Fig. 12 Temperature Distribution in the S/G with Semi-Flooded stator

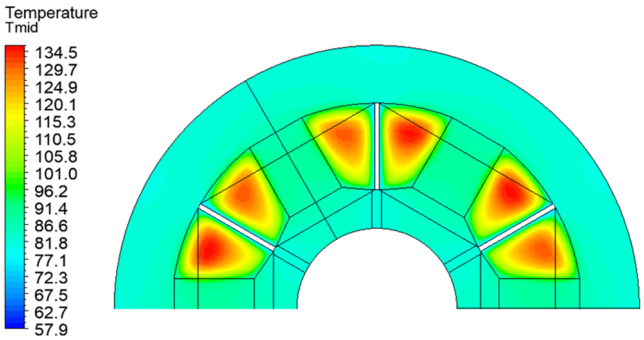

Fig. 13: Temperature Distribution in the Inductor with Semi-Flooded stator

Table VI summarise the temperature predicted using the two cooling approached discussed. As it can be noticed, a significant temperature reduction can be achieved, when using a direct cooling option; this can have a considerable impact on the power density achievable, on the efficiency and on the lifetime of the components. Last but not least, a further reduction of weight and volume can be also achieved, which is essential for aerospace applications.

TABLE VI:
MAXIMUM TEMPERATURES PREDICTED

Maximum Temperatures (°C)		
Component	Water Jacket	Direct Oil Cooling
Iron (S/G)	145	80
Iron (Inductor)	147	92
Copper (S/G)	148	82
Copper (Inductor)	212	135

VI. CONCLUSION

This paper presented a high current design of a passive filter inductor integrated within the common housing of the starter-generator. A series inductor was required to smooth out the switching ripple component from the current waveforms of the starter-generator. The inductor was sized using the area product approach followed by the finite element analysis which validated the electromagnetic performance of the integrated inductor. The total power losses at 8, 20, and 32 kRPM were evaluated to realise the thermal design of a combined starter-generator and integrated inductor system, while achieving the full integration from a thermal management point of view. A shared cooling configuration can guarantee safe operating conditions even at the most demanding operating points. The design proposed can significantly contribute to reduce the overall volume and weight of the system due to the lower number of hydraulic connections required. Low operating temperatures can also help to enhance the overall efficiency of the system

REFERENCES

[1] Robert Abebe, Gaurang Vakil, Giovanni Lo Calzo, Thomas Cox, Simon Lambert, Mark Johnson, Chris Gerada, Barrie Mecrow “Integrated motor drives: state of the art and future trends” IET Electric Power Applications, 15 pp, Print ISSN 1751-8660, Online ISSN 1751-8679

[2] M. Raza Khowja, C. Gerada, G. Vakil, P. Wheeler and C. Patel, "Integrated output filter inductor for permanent magnet motor drives," IECON 2016 - 42nd Annual Conference of the IEEE Industrial Electronics Society, Florence, 2016

[3] Muhammad Raza Khowja et al., "Novel Permanent Magnet Synchronous Motor with Integrated Filter Inductor, Using Motor’s Inherent Magnetics," IEEE Transactions on Industrial Electronics, 2020, In Press, DOI (identifier) 10.1109/TIE.2020.3000110

[4] M. R. Khowja et al., "Novel Motor-Shaped Rotational Inductor for Motor Drive Applications," IEEE Transactions on Industrial Electronics, vol. 67, no. 3, pp. 1844-1854, 2020.

[5] M. Raza Khowja, C. Gerada, G. Vakil, P. Wheeler and C. Patel, "Novel integrative options for passive filter inductor in high speed AC drives," IECON 2016 - 42nd Annual Conference of the IEEE Industrial Electronics Society, Florence, 2016

[6] M. Raza Khowja, C. Gerada, G. Vakil, C. Patel and P. Wheeler, "Design optimization of integrated rotational inductors for high-speed AC drive applications," 2017 IEEE International Electrical Machine & Drives Conference (IEMDC), Miami FL, USA, 2017

[7] M. Raza Khowja, C. Gerada, G. Vakil, C. Patel and P. Wheeler, "Design optimization of integrated rotor-less inductors for high-speed AC drive applications," 2017 IEEE Workshop on Electrical Machines Design, Control and Diagnosis (WEMDCD), Nottingham, United Kingdom, 2017

[8] M. Raza Khowja, C. Gerada, G. Vakil, S. Quadir Quadri, P. Wheeler and C. Patel, Design of an Integrated Inductor for 45kW Aerospace Starter-Generator," 2018 IEEE Transportation Electrification Conference and Expo (ITEC), Long Beach, CA, 2018, pp. 570-575.

[9] Colonel Wm. T. Mclyman “Transformer and Inductor Design Handbook”, Fourth Edition

[10] Kazimierczuk M.K, Sekiya H. “Design of AC resonant inductors using area product method” Energy Conversion Congress and Exposition, 2009. ECCE Bejan, A., Heat Transfer: Wiley 1993 1Th

[11] Staton, D.A. and A. Cavagnino, Convection Heat Transfer and Flow Calculations Suitable for Electric Machines Thermal Models. Industrial Electronics, IEEE Transactions on, 2008. 55(10): p. 3509-3516. 2Th

[12] Simpson, N., R. Wrobel, and P.H. Mellor, Estimation of Equivalent Thermal Parameters of Impregnated Electrical Windings. Industry Applications, IEEE Transactions on, 2013. 49(6): p. 2505-2515. 3Th

[13] A. La Rocca. Thermal Analysis of a High Speed electrical Machine, PhD Thesis, University of Nottingham, 2016 4Th

[14] Gaurav A., M.K., Sameer K., Thermo-hydrodynamics of developing flow in a rectangular mini-channel array, in Proceedings of Twentieth National and Ninth International ISHMT-ASME Heat and Mass Transfer Conference2010: